Supplementary material for:
"Calcium peroxide from ambient to high pressures"

J. R. Nelson, R. J. Needs and C. J. Pickard

Further information on the AIRSS searches

In our searches, we use a lower plane-wave basis cutoff of 500 eV and a coarser k-point sampling density of $2\pi\times0.07$ Å^{-1} along with ultrasoft pseudopotentials generated by the CASTEP code. Once low-enthalpy candidate structures have been identified, we proceed with the higher basis cutoff energy of 800 eV and k-point sampling density of $2\pi\times0.03$ Å^{-1}. All results presented in the main paper use this stricter set of parameters, with the exception of the oxygen structures, where a denser k-point sampling is needed owing to the metallic nature of some of its phases.

The number of structures relaxed during our AIRSS searches for CaO_2 structures are tabled below. Blank entries indicate that structure searching was not carried out for that combination of formula units and pressure.

In generating our starting cells for AIRSS, we require the starting cell to have at least 2 symmetry operations, in addition to having reasonable atomic bond lengths and a reasonable volume. The possibility of a triclinic phase of space group P1 (#1) for CaO_2 is therefore excluded by our searches. We justify this exclusion by appealing to symmetry: low-energy minima tend to correspond to symmetrical structures [1]. Hence it is unlikely that a P1 structure would give rise to a global minimum in enthalpy.

Formula units	0 GPa	10 GPa	20 GPa	50 GPa	100 GPa	150 GPa	200 GPa	Subtotal
1	460	272	292	340	496		549	2409
2	1111	283	280	1830	1553	1176	1210	7443
3	602	225	249	253	857		922	3108
4	1234	283	255	1288	1583	1325	1982	7950
5					94		235	329
6	360	250	280	278	580		644	2392
8	296	219	261	310	456		553	2095
							Total	25726

Equation of state for CaO_2

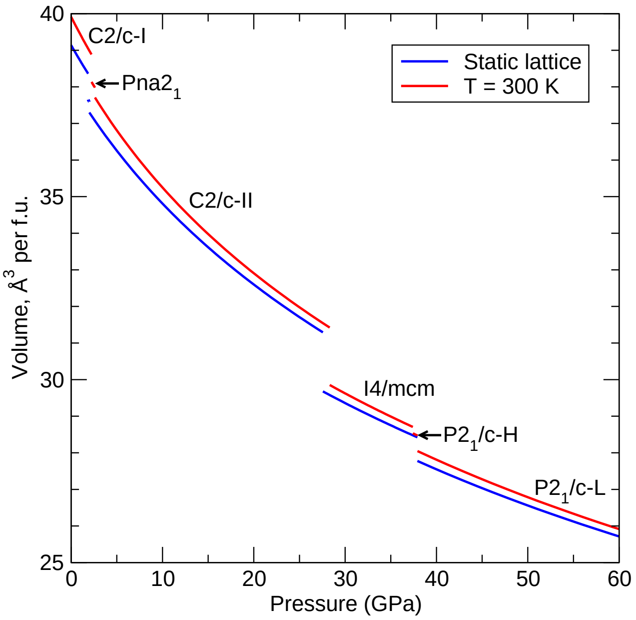

Fig. S1. The equation of state of calcium peroxide from the results of both our static-lattice calculations and phonon calculations at 300 K. The $P2_1/c$-H phase is not present in the static lattice equation of state, but is present over the small pressure range 37.4-37.9 GPa at 300 K.

Further electronic and phonon bandstructures

The bandgaps reported in the figure captions below are calculated using the PBE functional, so they will be underestimates of the true bandgaps.

$C2/c$-I-CaO$_2$

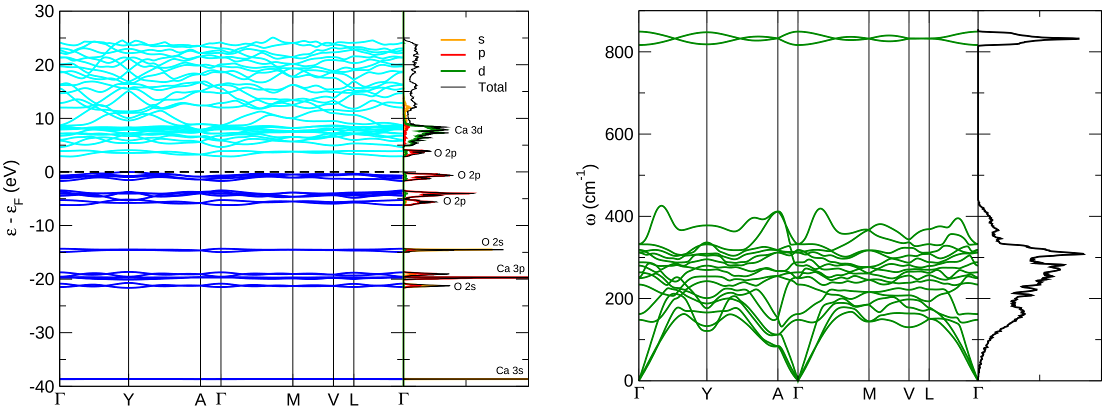

Fig. S2. Electronic bandstructure and density of states (*left*) for $C2/c$-I-CaO$_2$ at 0 GPa. We calculate a thermal bandgap of 2.9 eV and optical bandgap of 3.5 eV for this phase at 0 GPa. (*Right*) Corresponding phonon bandstructure and density of states.

$C2/c$-II-CaO$_2$

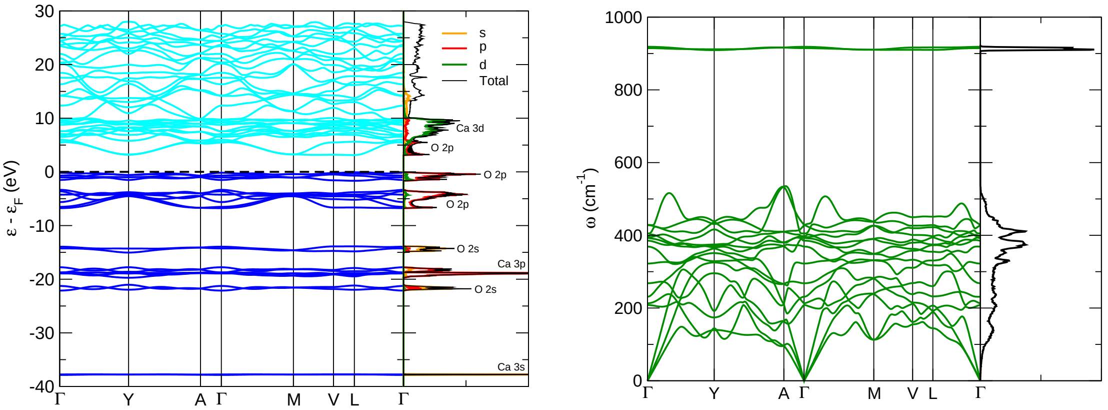

Fig. S3. Electronic bandstructure and density of states (*left*) for $C2/c$-II-CaO$_2$ at 20 GPa. We calculate a thermal bandgap of 3.2 eV and optical bandgap of 3.2 eV for this phase at 20 GPa. (*Right*) Corresponding phonon bandstructure and density of states.

$I4/mcm$-CaO$_2$

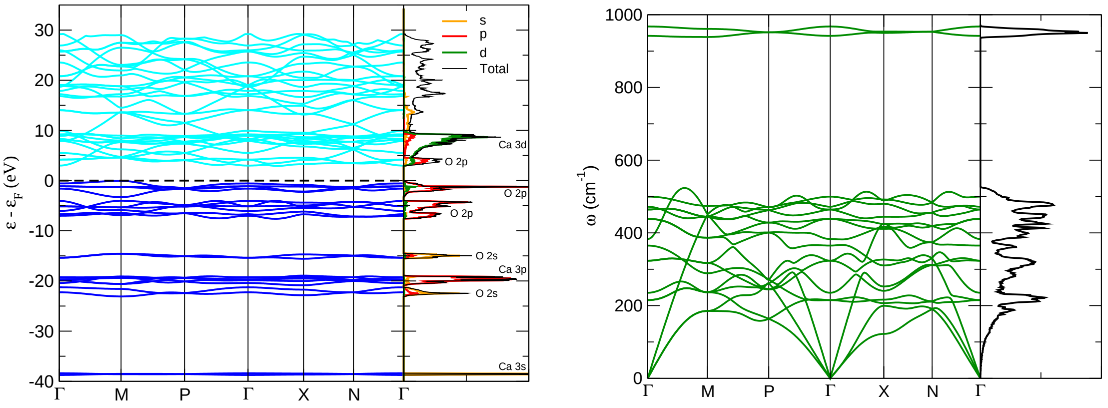

Fig. S4. Electronic bandstructure and density of states (*left*) for $I4/mcm$-CaO$_2$ at 30 GPa. We calculate a thermal bandgap of 3.0 eV and optical bandgap of 3.6 eV for this phase at 30 GPa. (*Right*) Corresponding phonon bandstructure and density of states.

$P2_1/c$-H-$\mathrm{CaO_2}$

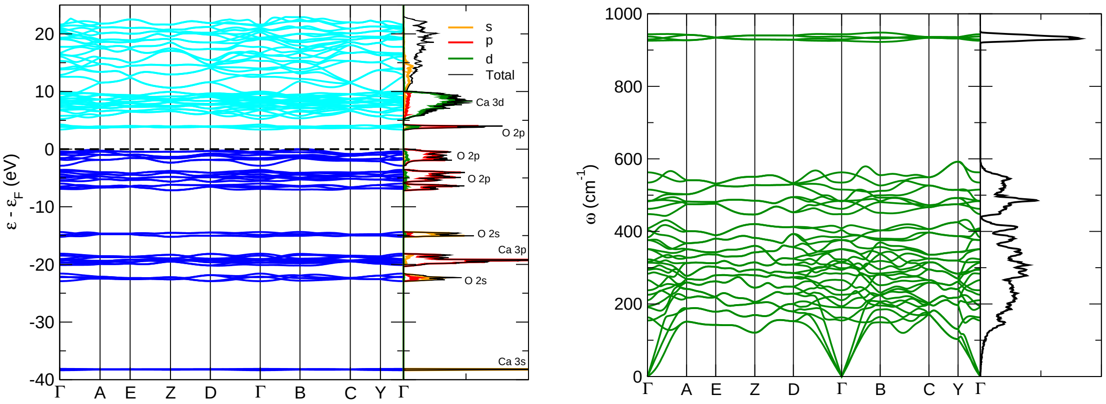

Fig. S5. Electronic bandstructure and density of states (*left*) for $P2_1/c$-H-$\mathrm{CaO_2}$ at 30 GPa. We calculate a thermal bandgap of 3.3 eV and optical bandgap of 3.6 eV for this phase at 30 GPa. (*Right*) Corresponding phonon bandstructure and density of states.

X-ray diffraction comparison of $C2/c$-I, $C2/c$-II and $Pna2_1$ structures

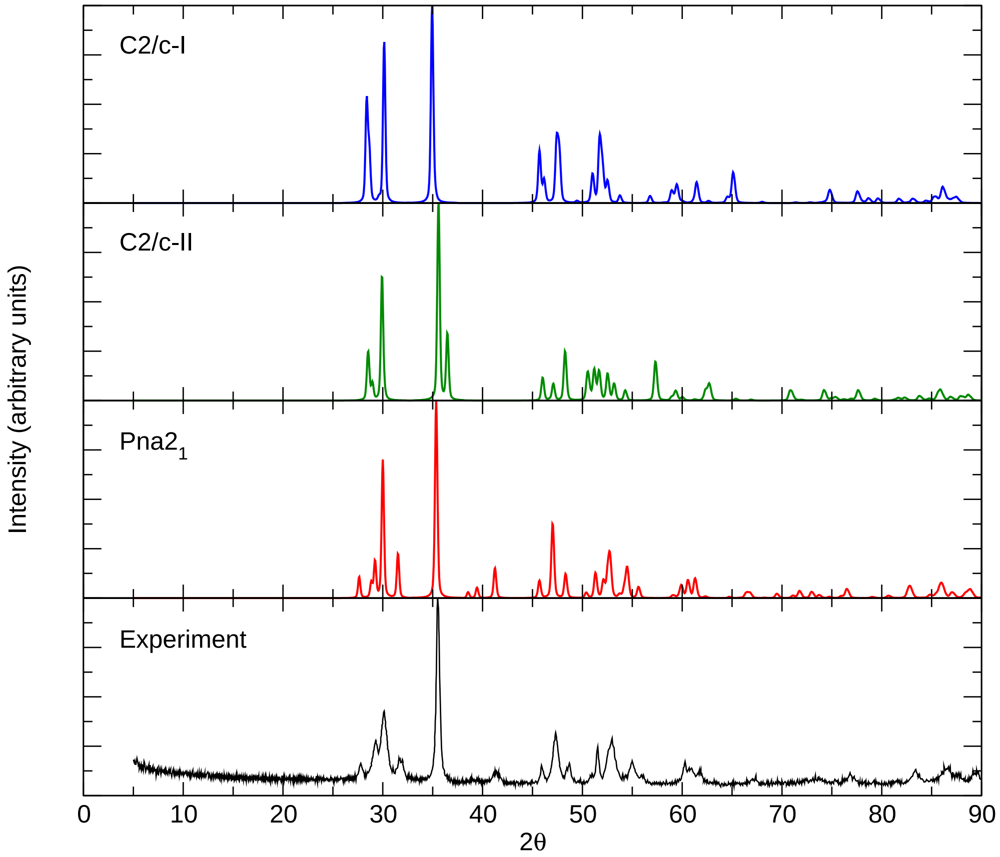

Fig. S6. Simulated powder XRD patterns (Cu, $\lambda = 1.540562$ Å) of the $C2/c$-I and $C2/c$-II phases of $\mathrm{CaO_2}$ (this work), as well as the $Pna2_1$ phase (after Zhao *et al.* [2]). The lower panel shows experimental data taken from Königstein *et al.* [3]. All simulated patterns are for DFT-relaxed structures at 0 GPa.

Further comparisons between the $C2/c$-I, $C2/c$-II and $Pna2_1$ phases

As mentioned in the main paper, the $C2/c$-I and $C2/c$-II phases of this work bear similarities to the $Pna2_1$ phase of CaO_2 found by Zhao *et al.* [2]. We discuss further the similarities and differences between these three phases here.

In Fig. S7, we show the $Pna2_1$, $C2/c$-I and $C2/c$-II phases as viewed down the crystallographic b-axis. This is (approximately) the view also used in Fig. 2 of the main paper. For the $Pna2_1$ phase, we orientate the a-axis to be horizontal on the page in Fig. S7, while the $C2/c$-I and $C2/c$-II phases are orientated so that $a+c$ (the [101] direction) is horizontal on the page.

From this perspective, calcium atoms form an almost-hexagonal pattern in the plane of the page, consisting of elongated diamonds with a peroxide ion at the center. A key difference between the structure of these three phases can also be seen - the peroxide ions in $C2/c$-I and $C2/c$-II are almost coplanar, whereas in $Pna2_1$ they form two sets of coplanar ions.

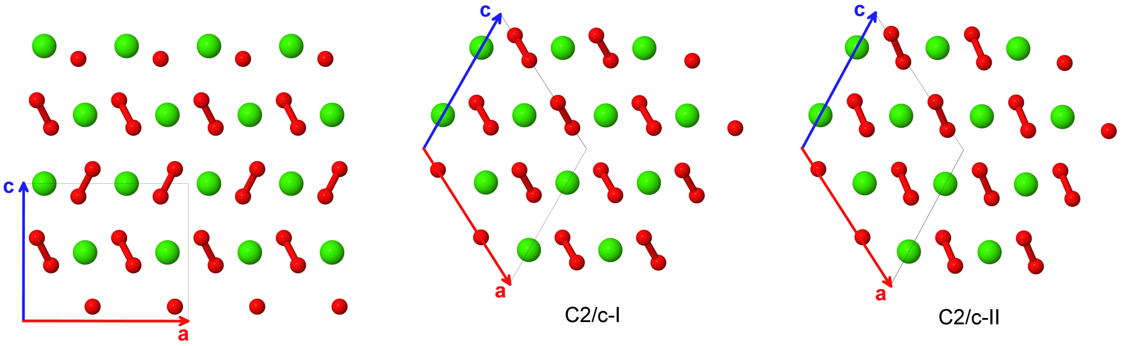

Fig. S7. The $Pna2_1$ (left, unlabelled), $C2/c$-I (middle) and $C2/c$-II (right) phases of CaO_2, as viewed down the crystallographic b-axis. The a-axis is horizontal and in the plane of the page for $Pna2_1$, while the $a+c$ axis is instead horizontal for $C2/c$-I and $C2/c$-II.

In Fig. S8, we show these three phases again, but viewed down the a-axis (for $Pna2_1$), and down the [101] direction (for $C2/c$-I and $C2/c$-II). This view is obtained by rotating the views of Fig. S7 by 90° about the vertical direction of the page.

From this perspective, the three phases are almost indistinguishable. Calcium ions form zig-zag rows running parallel to the a-axis ($Pna2_1$) and in the [101] direction ($C2/c$-I and $C2/c$-II).

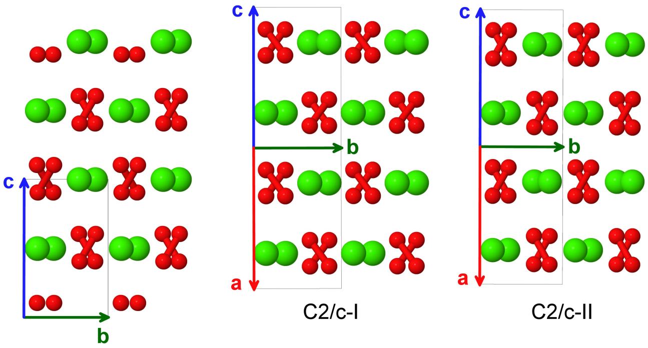

Fig. S8. The $Pna2_1$ (left, unlabelled), $C2/c$-I (middle) and $C2/c$-II (right) phases of CaO_2, as viewed down the crystallographic a-axis ($Pna2_1$), and the [101] direction ($C2/c$-I and $C2/c$-II).

Further illustrations of structures

$I4/mmm$-**CaO$_2$**

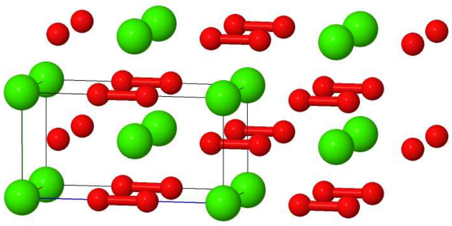

Fig. S9. The $I4/mmm$ structure of CaO$_2$. At 30 GPa, we have $a = b = 3.117$ Å, $c = 6.116$ Å; $\alpha = \beta = \gamma = 90°$; Ca atoms occupy the $2a$ (0,0,0) Wyckoff positions, and O atoms occupy the $4e$ (0,0,0.3800) Wyckoff positions. The enthalpies shown in Fig. 1 of the main paper are given relative to the enthalpy of this phase.

$I4/mcm$-**CaO$_2$**

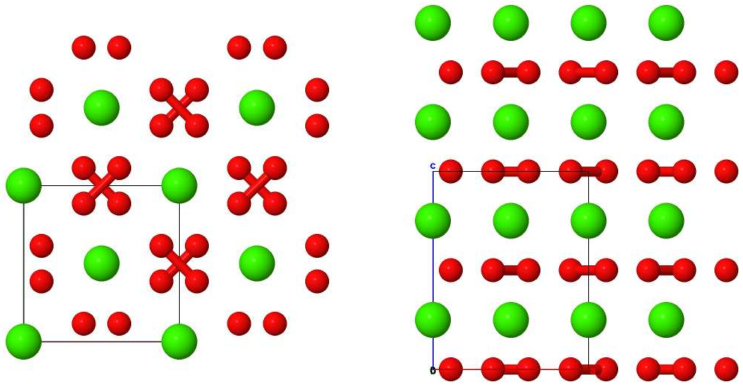

Fig. S10. (*Left*) View of the $I4/mcm$ structure of CaO$_2$, in the ab-plane. (*Right*) View in the ac-plane. At 30 GPa, we have $a = b = 4.521$ Å, $c = 5.745$ Å; $\alpha = \beta = \gamma = 90°$; Ca atoms occupy the $4a$ Wyckoff positions, and O atoms occupy the $8h$ (0.1143, 0.6143, 0.0000) Wyckoff positions as mentioned in Table I of the main paper.

On the pseudopotentials used in this study

The Center for Molecular Modelling [4] provides a database comparing pseudopotentials from a number of different plane-wave codes, including CASTEP (as used in this study). Pseudopotentials are benchmarked against all-electron full-potential calculations performed with the WIEN2K code. Pseudopotential performances are tested by examining the equations of state for pure element phases, and comparing the energy differences between pseudopotential and all-electron calculations.

The ultrasoft pseudopotentials that are generated by CASTEP version 8.0 have been tested in this manner, and show a root-mean-square deviation in energy from an all-electron calculation of just 0.5 meV/atom averaged across the periodic table. This difference is even smaller (0.06 meV/atom) for the calcium pseudopotential alone.

In our study, we used ultrasoft pseudopotentials generated by a slightly older version of CASTEP. Therefore, we test our pseudopotentials against the pseudopotentials of CASTEP-8.0, by comparing the calculated equilibrium lattice parameters and enthalpies of three different CaO$_2$ structures using our pseudopotentials, and the pseudopotentials of CASTEP-8.0. The PBE exchange-correlation functional is used for these tests. The table overleaf shows the results of these calculations.

$C2/c$-**I at 0 GPa**	Our pseudopotentials	CASTEP-8.0	Difference
Lattice a (Å)	7.0408	7.0388	+0.03%
Lattice b ($\equiv c$) (Å)	3.8761	3.8749	+0.03%
Lattice α (deg.)	123.233	123.242	−0.01%
Lattice β (deg.)	65.786	65.772	+0.02%
Lattice γ (deg.)	114.214	114.228	−0.01%
Enthalpy (meV/f.u.)[a]	−292.45	−291.04	−1.41
$C2/c$-**II at 20 GPa**	Our pseudopotentials	CASTEP-8.0	Difference
Lattice a (Å)	6.4067	6.4050	+0.03%
Lattice b ($\equiv c$) (Å)	3.8147	3.8135	+0.03%
Lattice α (deg.)	127.027	127.027	0.00%
Lattice β (deg.)	64.422	64.412	+0.02%
Lattice γ (deg.)	115.578	115.588	−0.01%
Enthalpy (meV/f.u.)[a]	−155.75	−155.06	−0.69
$P2_1/c$-H **at 30 GPa**	Our pseudopotentials	CASTEP-8.0	Difference
Lattice a (Å)	6.5896	6.5879	+0.03%
Lattice b (Å)	4.8424	4.8408	+0.03%
Lattice c (Å)	3.7946	3.7929	+0.04%
Lattice α ($\equiv \gamma$) (deg.)	90.000	90.000	(n/a)[b]
Lattice β (deg.)	105.248	105.252	−0.003%
Enthalpy (meV/f.u.)[a]	−86.62	−85.75	−0.86

[a] Relative to the $I4/mmm$ phase of CaO_2.

[b] These angles equal 90° by symmetry and are constrained as such.

We find a maximum enthalpy difference between the two sets of pseudopotentials of 1.41 meV/unit of CaO_2, while equilibrium lattice parameters differ by less than 0.04%. Given the above-mentioned accuracy of CASTEP-8.0 pseudopotentials compared to all-electron calculations, we expect that the pseudopotentials used in this study are able to accurately resolve energy differences between the CaO_2 phases we have considered.

References

[1] C. J. Pickard and R. J. Needs, J. Phys.: Condensed Matter **23**, 053201 (2011).

[2] X. Zhao, M. C. Nguyen, C.-Z. Wang and K.-M. Ho, RSC Advances **44**, 22135–22139 (2013).

[3] M. Königstein and C. Richard A. Catlow, J. Solid State Chem. **140**, 103–115 (1998).

[4] Center for Molecular Modelling: Comparing Solid State DFT Codes, Basis Sets and Potentials. Database online at `https://molmod.ugent.be/deltacodesdft`.